

Sound propagation in a Fermi gas near a Feshbach resonance

J. Joseph, B. Clancy, L. Luo, J. Kinast, A. Turlapov, and J. E. Thomas*
Duke University, Department of Physics, Durham, North Carolina, 27708, USA
(Dated: March 10, 2019)

Sound waves are observed and studied in an optically trapped degenerate Fermi gas of spin-up and spin-down atoms with magnetically tunable interactions. Measurements are made throughout the crossover region, from a weakly-interacting Fermi gas through the resonant Fermi superfluid regime to a Bose condensate of dimer molecules. The measured sound velocities test the equation of state and confirm the universal hypothesis.

Optically-trapped, strongly-interacting Fermi gases [1] provide a unique laboratory for testing nonperturbative many-body theories in a variety of fields, from neutron stars and nuclear matter [2] to quark-gluon plasmas [3] and high temperature superconductors [4]. In contrast to these other systems, interactions in ultra cold atomic Fermi gases are tunable using the Feshbach resonance phenomenon [5]: At magnetic fields well above the resonance, one obtains a weakly attractive Fermi gas, while well below the resonance, spin-up and spin-down atoms are joined into dimer molecules, which form a Bose-Einstein condensate (BEC) [6, 7, 8, 9]. On resonance, the gas is a strongly interacting Fermi superfluid [10].

The focus of this Letter is the precision measurement of the sound velocity at low temperatures in this unique quantum system. The experiment addresses the rich physics of wave propagation in a strongly-interacting system, such as possible coupling between first and second sound [11] and nonlinear behavior. We find that the wavefront is flat despite nonuniform density across the wavefront. This observation verifies the predicted relation [12] between the measured velocity in a cigar-shaped trap and the equation of state. As a result, by measuring the velocity we probe zero-temperature equations of state $\mu_{loc}(n)$, where μ_{loc} is the local chemical potential and n the total density of atoms. The equation of state is a central result of nonperturbative many-body theories that determine the thermodynamic parameters. Measurements at resonance over a wide range of densities confirm the universal hypothesis [1, 2, 13, 14] as well as the location of the Feshbach resonance [15].

The medium for the sound propagation is a 50:50 mixture of ${}^6\text{Li}$ atoms in the two lowest internal states or a BEC of Li_2 molecules near a broad Feshbach resonance centered at $B = 834$ G [15]. The gas is cooled by forced evaporation in an ultrastable CO_2 laser trap at the resonant magnetic field [1]. Near the end of evaporation, B is adiabatically set to a chosen final value between 700 and 1100 G, and the trap is adiabatically recompressed to a desired depth U_0 between 0.14 and 12 μK .

The experimental samples are nearly in the ground state, which can be determined from the absorptive images of the gas [1]. The gas is imaged after release from the trap and expanded to avoid saturation of images

due to high absorption. Close to unitarity and on the Fermi side of the Feshbach resonance, the density profiles can be closely approximated by the zero-temperature Thomas-Fermi profiles of a non-interacting Fermi gas. In the molecular BEC regime, the clouds do not have any observable thermal component, which appears when the cooling efficiency is significantly reduced. From the absorptive images we measure the total number of atoms N in the range 0.6 to 4.9×10^5 .

A sound wave is excited in the sample by the same method as used for a BEC of atoms [16]. A thin slice of green light bisects the cigar shaped cloud. The green light at 532 nm is blue detuned from the 671 nm transition in lithium, creating a knife which locally repels the atoms. The $1/e$ thickness of the knife is $\simeq 30 \mu\text{m}$. The height of the knife potential, U_{knife} , is estimated from the size, power, and atomic polarizability. U_{knife} is chosen to be between 0.5 and 14 μK . The knife is pulsed on for 280 μs , much shorter than typical sound propagation times ~ 10 ms. The resultant perturbation propagates outward along the axial coordinate z . We allow propagation for a variable amount of time and then release the cloud, let it expand for a fixed time, and image destructively. Propagation of the density perturbation is shown in Figure 1. The propagating feature consists of a region of low density (valley) with regions of high density (peak) on either side.

The main result of the Letter, shown in Figure 2, is the measurement of c_0/v_F , the normalized sound velocity in the center plane (at $z = 0$) vs $1/k_F a$, the dimensionless interaction parameter. The reference Fermi velocity v_F is that of a non-interacting Fermi gas at the trap center, i.e., $E_F = \hbar(\omega_x\omega_y\omega_z)^{1/3} (3N)^{1/3} = m_{atom}v_F^2/2 = \hbar^2 k_F^2/2m_{atom}$, where E_F is the Fermi energy and k_F is the corresponding Fermi wave vector. The trap frequencies ω_i are individually calibrated for each velocity measurement. At zero temperature, $1/k_F a$ is the only quantity that determines the physics. The s-wave scattering length $a = a(B)$ is estimated from Ref. [15]. At $|k_F a| \gg 1$ the system is in the strongly interacting regime and is a superfluid. The BEC (weakly interacting Fermi) regime corresponds to $1/k_F a > 1$ ($1/k_F a < -1$). We tune $k_F a$ by changing B and U_0 .

Five measures are taken to reduce systematic errors.

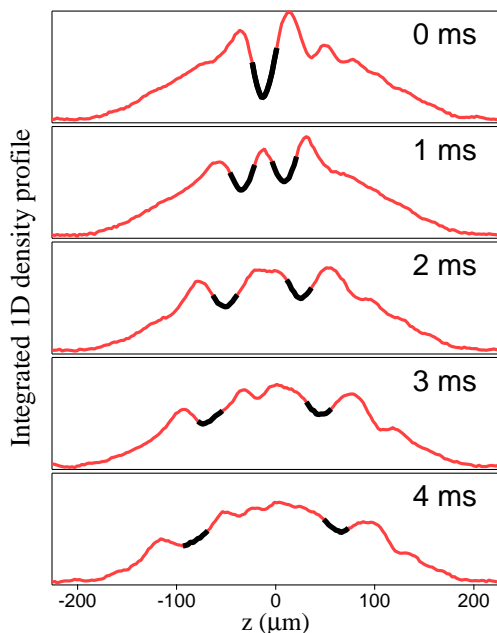


FIG. 1: Sound propagation at the Feshbach resonance: Integrated axial profiles of the cloud for different in-trap propagation times. Positions of the propagating density depressions (valleys) are highlighted. Propagation times are shown.

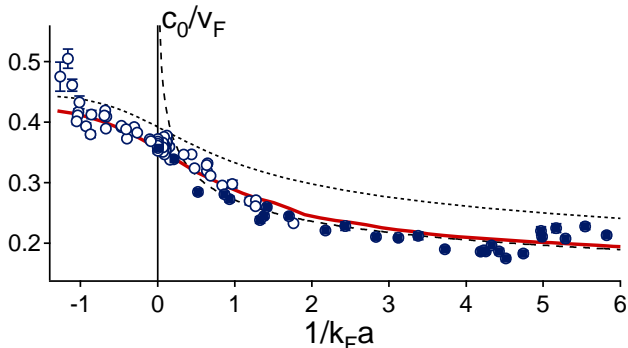


FIG. 2: Sound velocity in the center plane normalized to v_F vs the interaction parameter, $1/k_F a$. Black dotted curve – mean-field theory that uses the Leggett ground state [17]. Red solid curve – quantum Monte Carlo calculation [17]. Black dashed curve – Thomas-Fermi theory of a molecular BEC, using $a_{mol} = 0.6 a$. Open and closed circles represent ranges of trap depths, 0.6 to 12 μK and 140 to 410 nK, respectively.

First, by tracking both right- and left-propagating features (Fig. 3) we eliminate effects due to the overall motion of the cloud. Second, we correct for a small change of the axial cloud size between the release and imaging ($< 4.7\%$, 1.2% on average). In order to obtain in-trap positions of the propagating features, each imaged position is scaled by a coefficient of expansion calculated within a hydrodynamic model [1, 18].

Third, we account for the dependance of the velocity on the non-uniform density distribution along

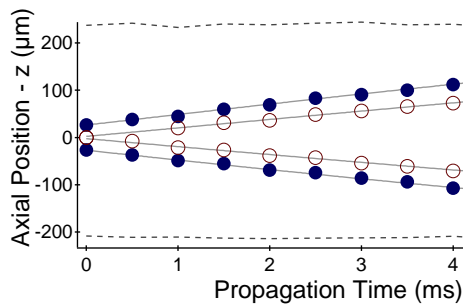


FIG. 3: Axial positions z of the left- and right-traveling density features of 1vs the in-trap propagation time. Coordinates of the valleys (blue-closed) and front peaks (red-open) are shown. Dashed lines correspond to the measured Fermi radii ($z = \pm R_z$).

z . Making a general approximation for the equation of state $\mu_{loc}(n) = C n^\gamma$ and calculating the velocity within using hydrodynamic theory [12, 19], one finds that $c(z) \propto \sqrt{1 - z^2/R_z^2}$ for a harmonically trapped gas, where R_z is the axial Thomas-Fermi radius. Then, one may show that a small density perturbation propagates as $z(t) = R_z \sin(\pm c_0 t/R_z + \varphi)$, where the phase $\varphi = \arcsin(z_{knife}/R_z)$ depends on the excitation position. c_0 , the velocity of the features at $z = 0$, is obtained by fitting the coordinates of the propagating features which lie within the central 65% of the cloud (Fig. 3).

Fourth, we account for nonlinearity in propagation: The front peak moves faster than the valley, as predicted earlier for BECs [20]. In Fig. 4, we show the velocities of the valley and peak vs the excitation strength, U_{knife}/μ , where μ is the global chemical potential estimated using Monte-Carlo modelling [17, 21]. The peak and valley

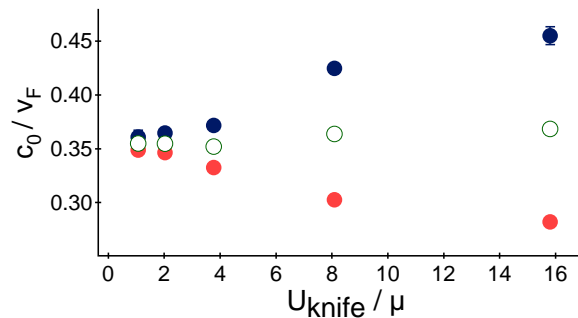


FIG. 4: Valley (red-closed) peak (blue-closed) and mean (green-open) velocity vs excitation potential normalized to the global chemical potential. Measured at the Feshbach resonance.

velocities vary with excitation strength, but the mean velocity remains constant. All velocities converge to a single value at low excitation strength showing that the mean accurately represents the velocity of an infinitely small perturbation. In reporting data, we use the mean

value. For data of Fig. 2, U_{knife}/μ ranges from 1 to 30. We do not observe formation of shock-waves which are predicted for a BEC [20].

Fifth, the data is corrected for anharmonicity of the trapping potential. We correct the measured sound velocities and find the velocity values which would be measured in a perfectly harmonic trap. Only the radial anharmonicity is taken into account because for shallow traps, in which the correction is greatest, harmonic magnetic confinement dominates axially. The radial confinement is optical, and the potential is gaussian. Axially, the potential is a sum of an optical and a parabolic magnetic potential with a common center ($\omega_z^2 = \omega_{z,opt}^2 + \omega_{z,B}^2$). The corrections for c_0 have been calculated to the first order in μ/U_0 from Eq. 1 below using either a Fermi ($\gamma = 2/3$) or Bose ($\gamma = 1$) equation of state $\mu_{loc} \propto n^\gamma$. The respective corrections are $c_0/c_0^{meas.} = 1 + 0.10 \mu/U_0$ and $c_0/c_0^{meas.} = 1 + 0.14 \mu/U_0$. The Fermi and Bose corrections have been used for $1/k_F a \leq 0$ and $1/k_F a > 1$. For $0 < 1/k_F a < 1$, these two corrections were linearly combined. μ/U_0 ranges from 0.025 to 0.43.

Precision characterization of the trap is important for calculating the reference Fermi speed v_F . The mean radial frequency $\omega_\perp = \sqrt{\omega_x \omega_y}$ is calculated from the radial breathing mode frequency ω_{breath} [22, 23], which is measured for each point of Fig. 2 on the day of the respective sound measurement. ω_{breath} is measured either at resonance, where $\omega_{breath} = \sqrt{10/3} \omega_\perp$, or in the far BEC regime, which yields consistent results. In the latter case, we assume $\omega_{breath.} = 2\omega_\perp$ neglecting a small beyond-mean-field correction [24, 25]. The ratio $\omega_x/\omega_y = 1.056$ and the total axial frequency ω_z has been measured using parametric resonance in a weakly-interacting Fermi gas [22]. The frequency of the magnetic field potential, $\omega_B/2\pi = 20.5$ Hz at 834 G, is measured using a sloshing mode. The trap anisotropy ratio ω_\perp/ω_z is between 4.1 and 25 depending on U_0 . For $U_0 = 6.1$ μ K, $\omega_\perp/2\pi = 690(2)$ Hz and $\omega_z/2\pi = 34.2(0.2)$ Hz. All radial frequencies have been corrected for anharmonicity [22, 23, 26]. The individual corrections to c_0 and v_F partially cancel when calculating the ratio c_0/v_F . The resulting correction to c_0/v_F is within 3.1% and, on average, is 0.7%.

Linking the speed of sound to the equation of state enables quantitative tests of theories. By analyzing the wave front shape we now show that the hydrodynamic model of Capuzzi et al. [12], for a cigar-shaped trap, provides a correct description of propagation. The primary result of this model is that the wave front stays flat, as described by

$$c(z) = \left(\frac{1}{m_{atom}} \frac{\int n dx dy}{\int (\partial \mu_{loc} / \partial n)^{-1} dx dy} \right)^{1/2}. \quad (1)$$

In contrast, a simple model of isotropic sound propagation assumes $c_{loc}(n) = \sqrt{(\partial P / \partial n) / m_{atom}}$, where P is the

pressure. In this case, the wave front curves as the wave propagates. For the same equation of state, these two theories predict a few per cent difference in the speed of the perturbation. In Figure 5 we experimentally demonstrate that the speed is independent of the transverse position, which validates Eq. 1 for our experimental conditions. And, hence, we can rely on Eq. 1 in connecting c_0 to $\mu_{loc}(n)$. At this point we are in a position to compare

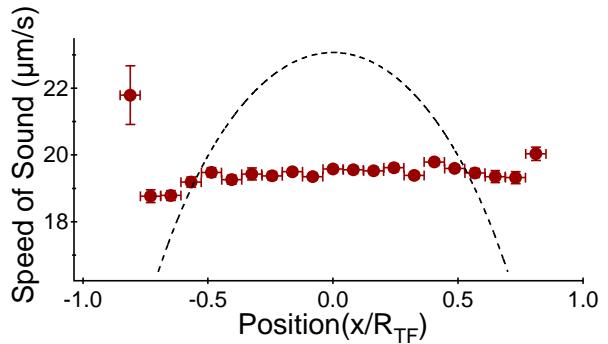


FIG. 5: Local sound velocity vs transverse coordinate x , in units of the Thomas-Fermi Radius, at the feshbach resonance showing flat wavefront. Images were divided into 21 longitudinal segments of equal width. For each i th segment, $c_i(z=0)$ has been measured. The dashed curve represents the line of site averaged isotropic sound speed.

the data of Fig. 2 to predictions.

In the BEC regime, at $1/k_F a > 1$, the experiment tests the interaction properties of composite bosons, molecules made out of two fermions. One may approximate the state of the gas as a BEC of singlet molecules that collide with s-wave scattering length a_{mol} . Using the local equation of state $\mu_{loc}(n_{mol}) = 2\pi\hbar^2 a_{mol} n / m_{mol}$ in Eq. 1, one finds $c_0/v_F = (5/2 k_F a_{mol})^{1/5} / 4$. An extension of the Leggett ground state into the Bose regime [27] gives $a_{mol} = 2a(B)$ resulting in a prediction for the speed 25 – 40% higher than measured. An exact solution of the four-fermion scattering problem predicts $a_{mol} = 0.6a$ [28] yielding a speed (black dashed curve in Figure 2) close to the measurements.

Theories covering the whole crossover from the Fermi to Bose regime can be tested against our data. In Fig. 2, the black dotted curve [17] represents the theory based on the Leggett ground state [27]. The theory predicts significantly higher speed than measured except for the Fermi side of the resonance. The red solid curve [17] shows the calculation that uses the equation of state obtained from a Monte-Carlo simulation [21]. This theory shows much better agreement with the data. Interestingly, in most of the molecular BEC regime, at $1/k_F a > 1$, the data is systematically lower than the prediction.

The lower measured speed at $1 < 1/k_F a < 5$ could be due to the coupling of first and second sound, which travels slower [11]. High temperature cannot be a reason for lower speed. We have found that higher tempera-

tures correspond to higher sound velocities. It is also unlikely that the speed is lower due to a dark soliton, which travel slower than sound, and, in principle may exist in our molecular BECs. The tracked density depressions are most likely not dark solitons for three reasons. First, unlike a dark soliton, the feature spreads out and loses contrast with time (Fig. 1), which is observed at all $1/k_F a$'s. Second, the soliton size is predicted to be of the same order as the coherence length [29], $\hbar/\sqrt{2\mu m_{mol}} < 1 \mu\text{m}$, while the imprinted density depression has the width of $10 - 20 \mu\text{m}$. Third, the optimum soliton excitation requires phase imprint of π [30], while in our experiment, the phase imprint for most of the BEC-side experiments is $\simeq 20\pi$.

The small speed increase at $1/k_F a > 5$ could occur due to a technical reason: To achieve these high $1/k_F a$ values we have to use very shallow traps. The BECs released from these weakest traps are small and difficult to image.

The universal hypothesis is positively tested in our measurements. The hypothesis states that at resonance, where $k_F a = \infty$, c_0/v_F should be independent of density. Indeed, within the experimental precision, at resonance, at 834(2)G, we observe that c_0/v_F remains constant as the trap depth is changed from 410 nK to 12 μK . In contrast, below the Feshbach resonance, at 821 G, c_0/v_F decreases with decreasing U_0 . These measurements of c_0/v_F vs U_0 show that the Feshbach resonance location is much closer to 834 G than to 822 G [31].

From the sound velocity at resonance, we have also measured the universal constant β [1, 2], which connects the local interaction and Fermi energy in the universal regime: $U_{int} = \beta \epsilon_F$. Using $\mu_{loc} = \epsilon_F + U_{int} = (1 + \beta) (3\pi^2 n)^{3/2} \hbar^2 / 2m_{atom}$ and Eq. 1, one may relate c_0 to β as:

$$\frac{c_0}{v_F} = \frac{(1 + \beta)^{1/4}}{\sqrt{5}}, \quad (2)$$

from which we find $\beta = -0.570(0.015)$.

On the far Fermi side of the Feshbach resonance, at $1/k_F a < -1.3$, propagation of sound is not observed. Instead, the hole from the laser knife fills without propagating, as in a non-interacting gas. At the temperatures we achieve, the gas is not necessarily a superfluid in the weakly interacting Fermi gas region, and hydrodynamic sound propagation is provided by collisional, rather than superfluid hydrodynamics.

In conclusion, we have observed sound propagation, connected observations to a hydrodynamic model, and provided data for testing theories describing strongly-interacting Fermi systems as well as their crossover into the weakly interacting Fermi and Bose regimes.

We thank G. Astrakharchik, P. Capuzzi, L. Carr, K. Levin, Qijin Chen, Yan He, K. Machida, and T. Ghosh

for stimulating discussions and correspondence. This research is supported by the Physics Divisions of the Army Research Office and the National Science Foundation, the Physics for Exploration program of the National Aeronautics and Space Administration, and the Chemical Sciences, Geosciences and Biosciences Division of the Office of Basic Energy Sciences, Office of Science, U. S. Department of Energy.

* jet@phy.duke.edu

- [1] K. M. O'Hara, et al., *Science* **298**, 2179 (2002).
- [2] H. Heiselberg, *Phys. Rev. A* **63**, 043606 (2001).
- [3] P. F. Kolb and U. Heinz, *Quark Gluon Plasma 3* (World Scientific, 2003), p. 634.
- [4] Q. Chen, et al., *Phys. Rep.* **412**, 1 (2005).
- [5] M. Houbiers, et al., *Phys. Rev. A* **57**, R1497 (1998).
- [6] S. Jochim, et al., *Science* **302**, 2101 (2003).
- [7] M. Greiner, C. A. Regal, and D. S. Jin, *Nature* **426**, 537 (2003).
- [8] M. W. Zwierlein, et al., *Phys. Rev. Lett.* **91**, 250401 (2003).
- [9] T. Bourdel, et al., *Phys. Rev. Lett.* **93**, 050401 (2004).
- [10] M. Zwierlein, et al., *Nature* **435**, 1047 (2005).
- [11] H. Heiselberg, *Phys. Rev. A* **73**, 013607 (2006).
- [12] P. Capuzzi, et al., *Phys. Rev. A* **73**, 021603(R) (2006).
- [13] T.-L. Ho, *Phys. Rev. Lett.* **92**, 090402 (2004).
- [14] J. E. Thomas, A. Turlapov, and J. Kinast, *Phys. Rev. Lett.* **95**, 120402 (2005).
- [15] M. Bartenstein, et al., *Phys. Rev. Lett.* **94**, 103201 (2005).
- [16] M. R. Andrews, et al., *Phys. Rev. Lett.* **79**, 553 (1997).
- [17] G. Astrakharchik, private communication.
- [18] C. Menotti, P. Pedri, and S. Stringari, *Phys. Rev. Lett.* **89**, 250402 (2002).
- [19] T. K. Ghosh and K. Machida, *Phys. Rev. A* **73**, 013613 (2006).
- [20] B. Damski, *Phys. Rev. A* **69**, 043610 (2004).
- [21] G. E. Astrakharchik, et al., *Phys. Rev. Lett.* **93**, 200404 (2004).
- [22] J. Kinast, et al., *Phys. Rev. Lett.* **92**, 150402 (2004).
- [23] J. Kinast, A. Turlapov, and J. E. Thomas, *Phys. Rev. A* **70**, 051401(R) (2004).
- [24] G. E. Astrakharchik, et al., *Phys. Rev. Lett.* **95**, 030404 (2005).
- [25] A. Altmeyer, et al. (2006), arXiv:cond-mat/0609390.
- [26] These frequency shifts were derived by S. Stringari, private communication. In the molecular BEC regime, $\omega_{breath.}/2\omega_{\perp} = 1 - 7/6 m\omega_{\perp}^2 x_{rms}^2/U_0$.
- [27] P. Nozières and S. Schmitt-Rink, *J. Low Temp. Phys.* **59**, 195 (1985).
- [28] D. S. Petrov, C. Salomon, and G. V. Shlyapnikov, *Phys. Rev. Lett.* **93**, 090404 (2004).
- [29] A. Jackson, G. M. Kavoulakis, and C. J. Pethick, *Phys. Rev. A* **58**, 2417 (1998).
- [30] S. Burger, et al., *Phys. Rev. Lett.* **83**, 5198 (1999).
- [31] C. H. Schunck, et al. (2004).